2020 3rd IEEE International Conference on Soft Robotics (RoboSoft)
Yale University, USA

Closing the Loop with Liquid-Metal Sensing Skin for Autonomous Soft Robot Gripping

Jessica Yin[1], Tess Hellebrekers[2] and Carmel Majidi[1,2]

***Abstract*— Soft robots are often limited in high-level decision making and feedback control due to a lack of multimodal sensing capabilities and material architectures that tightly integrate sensing and actuation. However, the recent development of elastic multimodal sensing skins has created the opportunity for closing the loop in soft robotic systems. In this work, we present a sensor-based finite state machine for a soft sensorized gripper mounted to a 4-degree-of-freedom robot arm. The soft gripper actuates between binary open and close states by activating shape-memory alloy springs, and contains proximity, pressure, and orientation sensors. The closed-loop control is demonstrated through scanning, grasping, and sorting tasks driven by sensor feedback. Using a time-of-flight distance sensor, the system can calculate the length, width, height, and center of mass of an object within a 60 mm x 25 mm workspace. With the time-of-flight distance sensor, pressure sensors, and inertial measurement unit, the system can detect and respond to external perturbations that interfere with the grasp, release, and transport of the object. The control strategy demonstrated in this paper can be expanded in the future to integrate basic autonomy in other soft robot systems.**

I. INTRODUCTION

Progress in broader applications of soft robots relies on the development and implementation of autonomy and decision-making in soft robotic systems. Armed with the capability for sensor feedback control, soft robots can begin to solve more complex problems and work towards levels of sophistication common in conventional rigid robotics. However, current limitations in multimodal soft sensing skins and soft electronics integration has resulted in sparse development of closed-loop control for soft robots [1], [2]. In addition, the deformable and compliant bodies of soft robots that make them so compelling in applications in healthcare, human-robot interaction, and bio-inspired robotics have presented a significant challenge in the development of dynamic control algorithms [3], [4]. While the compliance of soft robot bodies can negate the need for precise feedback control in interactions with the environment and delicate objects, sensor feedback is still necessary for higher level decision-making.

New developments in soft sensing technology in recent years have led to a greater availability of sensing modalities in soft robots than ever before. The functionality of these novel sensors has been thoroughly tested and characterized, but it is less common to see these novel sensors integrated into full soft robotic systems and applied to robotic tasks.

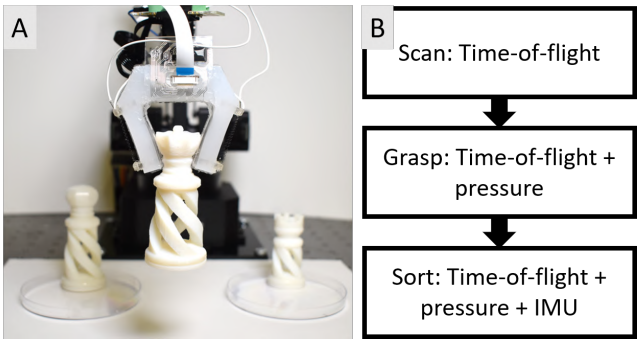

Fig. 1. A) Binary soft gripper actuated by shape-memory alloy with on-board sensor skin sorting objects by height. B) Overview of system states and their relevant sensor feedback used during tasks.

In this paper, we present the closed-loop control of a soft robotic system consisting of a sensorized soft gripper, 4-degree-of-freedom (DOF) robot arm, and finite state machine (Figure 1A). The multimodal sensing skin of the soft robot provides a time-of-flight distance sensor (ToF), inertial measurement unit (IMU), and two pressure sensors. These sensors govern the state of the finite state machine throughout scanning, grasping, and sorting tasks (Figure 1B).

II. RELATED WORK

Approaches to soft actuation can be broadly divided into the following categories: pneumatic, cable-driven, shape memory alloys, and electroactive polymers [5]. These actuation methods have been successfully applied to a variety of soft systems, including grippers [6], bio-inspired robots [7], and locomotion robots [8]. Approaches to soft sensing include resistive and capacitive stretchable sensing [9], [10], magnetic sensing [11], [12], and optoelectronic sensing [5], [13], [14]. Taking it one step further, progress has also been made in multimodal soft sensors, such as a thermal and humidity sensing graphene electronic skin [15], and a strain and pressure sensing skin [16].

The next challenge is developing systems that integrate both soft sensors and actuators together. Common strategies include adhering a soft sensing skin to the outside surface of the robot [17] and embedding sensors directly into the robot body [18], [19], [20]. Sensing skin and actuator integration can most frequently be seen in soft robotic grippers [21], [22], [23], [24], [25].

*This work was in part supported by the National Science Foundation (NSF) Graduate Research Fellowship Program (GRFP) under Grant No. DGE 1252522 and the National Oceanographic Partnership Program (NOPP) under Grant No. N000141812843 (PM: Dr. Reginald Beach). Any opinions, findings, and conclusions or recommendations expressed in this material are those of the author(s) and do not necessarily reflect the views of the NSF or NOPP.

[1]Department of Mechanical Engineering, Carnegie Mellon University, Pittsburgh PA 15213

[2]Robotics Institute, School of Computer Science, Carnegie Mellon University, Pittsburgh PA 15123, USA

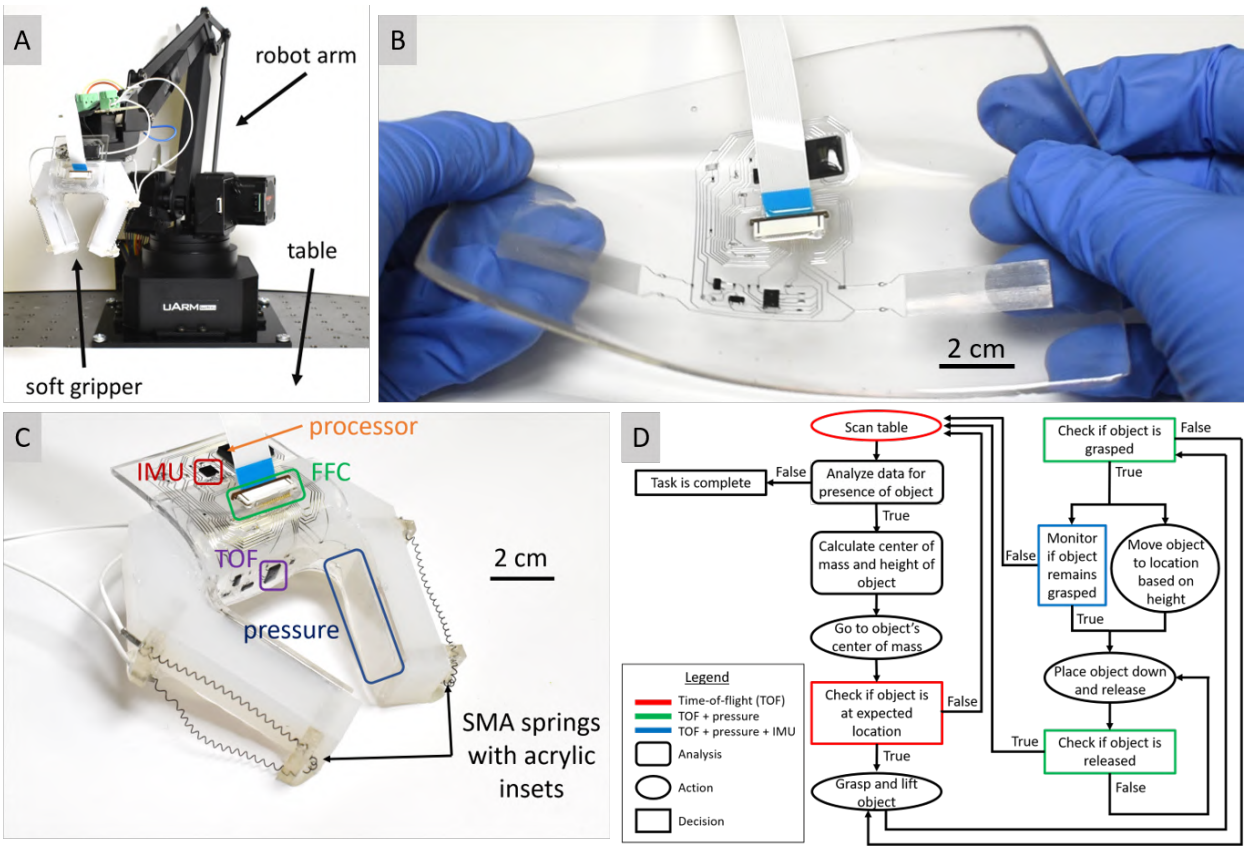

Fig. 2. A) Overview of experimental set-up with robot arm, sensorized soft gripper, and table for scanning. B) Soft and stretchable sensor skin with liquid-metal traces and embedded rigid microelectronics. C) Overview of sensorized soft gripper with sensors in relevant locations. D) Detailed block diagram of finite state machine to sort objects based on height.

However, despite progress in material architectures for integrated soft robot sensing and actuation, there are only a few systems to-date that use soft actuation and sensing together for high-level tasks. One possible reason for this might be the difficulty of fabricating larger-scale soft robotic systems that are adequately robust and seamlessly integrated. Nonetheless, there are examples of systems that successfully use soft actuation and sensing for high-level decision making. These include an optoelectronically innervated prosthetic hand used to select ripe tomatoes based on shape and softness [26] and a pneumatically actuated gripper capable of screwing in a light bulb [27].

We build upon previous work to contribute to the exploration of this systems integration space. We have previously demonstrated a hybrid soft sensor skin capable of orientation, pressure, temperature, and proximity sensing in which the signals are processed on-board [28]. The hybrid soft sensor skin was integrated with a shape-memory actuated soft gripper, and the performance of the sensors and gripper was characterized. While the current paper uses a similar sensor skin and gripper, we build upon the work by demonstrating signal feasibility in high-level robotic tasks. Specifically, we demonstrate closed-loop control of a soft robotic system with integrated sensing, processing, and actuation in scanning, grasping, and sorting tasks. The successful use of a finite state machine for closed-loop control of this system indicates that existing control strategies for rigid robots may also be applicable to soft robots.

III. EXPERIMENTAL SETUP AND FABRICATION

The sensorized gripper is attached to a 4-DOF robot arm (uArm Swift Pro; uFactory) (Figure 2A). The robot arm is connected to the computer hosting the finite state machine via serial communication. The robot arm is programmed with five actions: scan, grasp, lift, transport, and release.

A. Sensorized Gripper

The sensorized gripper is composed of two SMA-actuated elastomer fingers that are coated with a sensing skin. The sensor skin is embedded with two resistive pressure sensors (EGaIn: 75% Ga and 25% In, by wt), IMU (MPU9250; InvenSense), time-of-flight range sensor (VL6180X; ST Microelectronics), and a processor (Simblee; RFDigital) for signal processing and data transmission (Figure 2B, 2C). A 0.5mm pitch flat flexible cable (FFC) connector provides power and serial communication for reprogramming the processor and streaming the data. These components were selected to provide relevant sensing for gripping tasks and were placed in locations according to their sensing functionality. The ToF chip is placed in the 'palm' of the gripper parallel to the scanning surface, to measure the approximate distance to the

object. This data is used to determine the approximate size, location, and height of the object during scans, as well as the presence of the object in the grasp of the gripper during transport, grasp, and release actions. The resistive pressure sensors are composed of microfluidic channels of eutectic gallium-indium (EGaIn) liquid metal (LM) alloy [25] and are placed along each finger of the gripper to detect contact with the object. An IMU is located at the top front face of the gripper to determine if an external physical force was exerted on the gripper. LM traces connect the microelectronic components and polydimthylsiloxane (PDMS; 10:1 base-to-curing agent ratio; Sylgard 184; Dow Corning) is used to form the base and sealing layers of the sensor skin. Lastly, the sensor skin is adhered to the soft gripper with a silicone adhesive (Silpoxy; Smooth-On Inc.).

The soft gripper is fabricated from soft silicone (Dragon-skin 30; Smooth-On Inc.) and actuated using shape memory alloy (SMA) springs (Dynalloy, Inc.). The liquid elastomer is poured into a 3D-printed mold (Objet 24; Stratasys) to form the main body of the gripper. Acrylic insets to attach the SMA springs and mount to the robot arm are inserted into the mold prior to curing. The SMA springs contract due to Joule heating when powered with electrical current (0.64A) to open the gripper. When the DC current is removed, the SMA springs relax and the gripper closes. This design minimizes power consumption by passively holding objects and only requiring power to open the gripper. Complete details of the fabrication process and integration technique for creating the soft gripper, sensing skin, and EGaIn-based circuitry are presented in [28], [29].

B. Gripper and Arm Integration

The sensorized gripper provides data that informs the robot arm's motion and decision-making. First, the arm scans over a designated workspace with the ToF data to locate the object for grasping. A successful grasp is verified by both the proximity and pressure data. The proximity, pressure, and orientation data is continuously monitored to ensure successful transport and release of the object.

The scan consists of a 2D sweep over a 60mm x 25mm area in 6 uniform rows at a constant height of 100mm. This height of 100mm for the gripper throughout FSM states was chosen with consideration to the range of motion of the robot arm, the range of the ToF sensor, and the expected dimensions of the objects in the data set. Each row in the width axis is separated by 5mm. The robot arm moves 60mm at 1.4mm/s lengthwise while the sensorized gripper collects data, and returns to the starting position of each row at 60mm/s when the gripper is not collecting data.

The grasp begins with the robot arm moving to the position directly above the object's calculated center of mass, as determined by the ToF data. The robot arm then activates the SMA springs to open the gripper and lowers the gripper towards the object. The distance that the robot arm lowers the gripper is determined by the height classification of the object. These distances were calibrated to objects used in our specific demonstration of the system (further discussed in Section VI), and can be changed for interactions with objects of different dimensions. The height classification is based on a threshold value calibrated to the object dimensions that the gripper is expected to encounter and generated from the ToF scan data. Once the gripper is lowered, the SMA springs are deactivated to allow the gripper to close. After the grasp is completed, the robot arm lifts the gripper to the appropriate height for transport.

In transport, the arm moves the object to a specified position on the tabletop. This position is determined by the height classification of the object and the number of objects with the same height classification that were previously sorted. The release begins with lowering the gripper to a specific distance determined by the height classification of the object to place the object on the tabletop without damaging it. The SMA springs are activated to open the gripper and release the object. The SMA springs remain activated until the gripper returns to the height for transport. Then, the SMA springs are deactivated and the gripper closes.

The robot arm features two Grove (Seeedstudio) ports for modulating power and control signals that are delivered to the external modules at the end-effector. In our system, the signal pin is used with an n-channel MOSFET and DC current source to control the activation of the SMA springs from one Grove port, while the SMA springs are powered by the DC current in the other Grove port.

IV. Finite State Machine

A finite state machine (FSM) was selected as the control system to demonstrate basic autonomy and feedback control. The tasks of scanning, grasping, and sorting demonstrated on this system are well-suited to FSM control because the tasks can be distinctly divided into a relatively small number of states directly determined by sensor data. The FSM has six states: scan, move to the calculated center of mass of the object, lower the arm to attempt grasping the object, lift, sort, and release (Figure 2D).

A. Scan

In the scan state, the FSM commands the arm to move across the scanning area while the ToF data is collected and stored in a 2D array. After the scan is complete, the data is analyzed as an image with OpenCV to determine the approximate size, center of mass location, and height classification of the object (Figure 3). Because the approximate distance from the ToF sensor to the tabletop is known, any distance measurement greater than a numerical threshold is identified as part of the object. The arm is set to scan at a height of 100mm, and the distance measurements of the ToF scanning the tabletop unoccupied by an object range from 100mm to 118mm. In our system, the threshold value is 98mm to provide a buffer for potential sensor noise.

If there are no distance measurements that pass the threshold to be classified as part of an object, then the FSM concludes that there are no more objects and terminates. When the FSM terminates, the gripper and arm remain stationary at the starting position of a scan and the Python

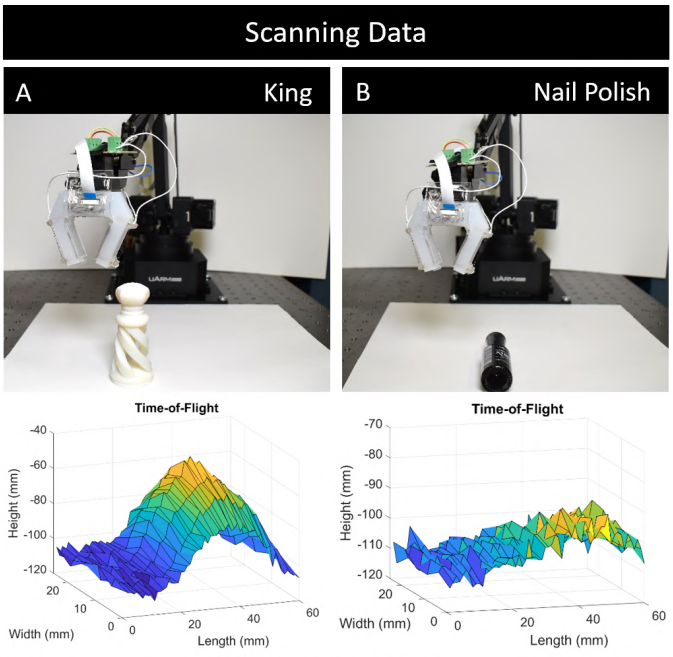

Parameter	Calculation
Size	42mm x 25mm
Location (G-code coordinates)	[242, -19]
Height	51mm
Classification	Tall

Parameter	Calculation
Size	36mm x 25mm
Location (G-code coordinates)	[246, -26]
Height	27mm
Classification	Short

Fig. 3. 3D ToF scan and parameters calculated by system from data of A) king chess piece and B) nail polish.

program containing the FSM is exited. If the approximate size of the object is determined to be too large or too small to be successfully grasped by the gripper, the FSM will re-scan the area up to four times before terminating. The additional scans are to account for potential miscalculation of object size from sensor noise or inaccurate data caused by varied ambient light conditions. If the object's approximate size is within the range that can be successfully grasped by the gripper, the FSM proceeds to the next state: move to the calculated center of mass of the object.

B. Move to Calculated Center of Mass

To calculate the location of the center of mass, the object is assumed to be rectangular, and the length and width are divided in half. The data points are scaled to mm units (1 data point:1mm length, 1 data point:5mm width) and converted to G-code coordinates (Figure 3). The arm then moves to the calculated location and uses a live stream of ToF data to determine if the object is at the expected location. Because the gripper is not able to successfully grasp objects shorter than 17mm, as found through experimentation, we assume that all objects that the gripper will encounter are taller than 17mm. Thus, the threshold value for classifying an object as present is 83mm. If the ToF distance measurement at that position is less than 83mm, the object is designated as present at the location and the FSM proceeds to the next state of attempting to grasp. If the ToF distance measurement at that position is greater than 83mm, i.e. the object is not present at that location, the FSM returns to the scan state.

C. Grasp

The FSM commands the arm to execute the grasp action based on the object's height measurement found in the scan state. The height measurement is used to classify the object as either short or tall to determine how far to lower the gripper. Once the grasp is completed, the FSM uses the live stream of pressure and ToF data to determine if the object has been successfully grasped. A successful grasp is defined using threshold values for the pressure and ToF sensors: a decrease by 1 or more Ohms in the resistive pressure sensors and a distance of less than 25mm from the TOF (Figure 4). These threshold values were experimentally derived from data collected during successful grasps of objects made from rigid materials, such as glass and 3D printed photopolymer (VeroWhite; Stratasys). If the grasp is successful, the FSM will move on to the next state. If the grasp is unsuccessful and the object is still sensed to be at that location, the FSM will re-attempt grasps up to four more times before terminating. If the grasp is unsuccessful and the object is detected as absent from that location, the FSM will return to the scan state.

D. Lift

The FSM commands the arm to execute the lift action. Once the lift is completed, the live stream of ToF and pressure sensor data is used to check if the object is in the grasp of the gripper, using the same threshold values defined in a successful grasp. If the object remains in the grasp of the gripper, the FSM proceeds to the next state. If the object is detected as not present, the FSM returns to the previous state and attempts to grasp the object again.

E. Sort

Using the object's height classification from the scan state, the FSM selects the location that the object should be placed and commands the arm to transport the object. During the arm's movements, the FSM monitors if the object remains in the grasp of the gripper by using thresholds of the IMU, ToF, and pressure sensor data. The IMU data stream is monitored for abnormal changes in measurements of the roll, pitch, and yaw that would indicate a perturbation to the system. The ToF's and pressure sensors' data stream is monitored throughout transport for the same threshold values as previously defined for a successful grasp. If the object is removed during transport, the FSM will return to the scan state. If the object is detected to have remained in the grasp of the gripper to the completion of the transport motion, the FSM proceeds to the next state.

F. Release

The FSM directs the arm to execute the release action. A successful release of the object is determined by the same threshold values from the ToF and pressure sensor data in detecting the successful grasp of the object (Figure 4). If

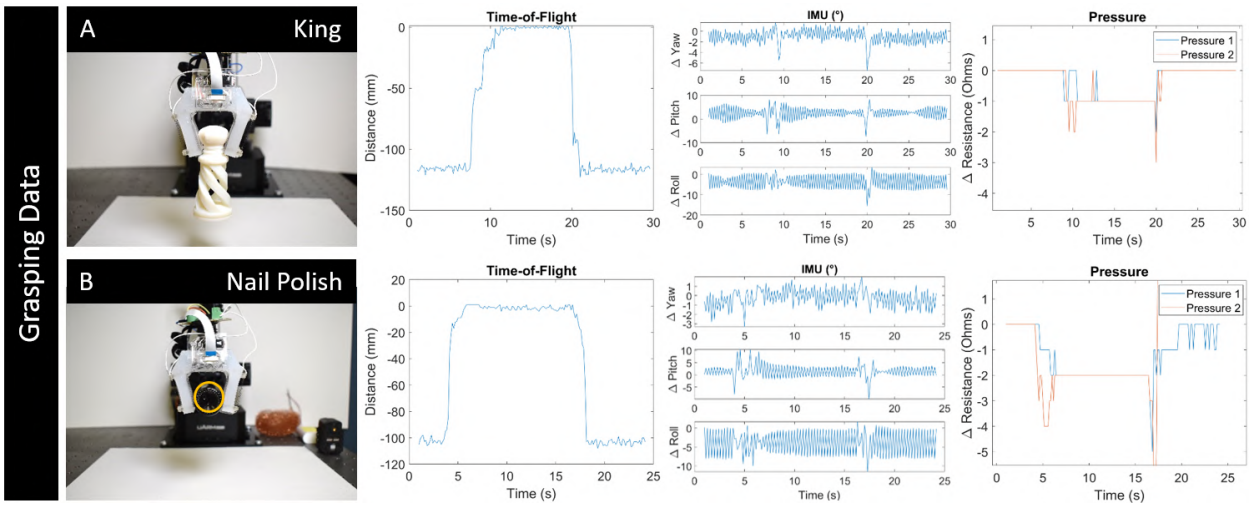

Fig. 4. Data outputs from time-of-flight, IMU, and pressure sensors during single grasp and release of A) king chess piece and B) nail polish.

the release is determined to be unsuccessful, the gripper will attempt to release the object up to four more times before deciding that the object cannot be successfully released. The FSM will then terminate. If the release of the object is successful, the FSM returns to the scan state to search for more objects.

TABLE I

SUCCESS RATE (%) IN UNPERTURBED OPERATION OVER 25 TRIALS.

Item	Locate	Classify	Grasp	Transport	Release
Rook	100	92	92	88	84
King	100	100	100	84	84

V. RESULTS AND DISCUSSION

We demonstrate the functionality of a soft robotic system consisting of a FSM, sensorized soft gripper, and robot arm that is: (i) robust to perturbations that interfere with grasping, transport, and sorting tasks; (ii) able to detect, classify, and locate objects within its scanning workspace; and (iii) capable of sorting a sequence of objects based on height. The soft robotic system is autonomous within constrained environments. The threshold values used for decision-making are relevant to specific objects but can be adjusted accordingly for other datasets. From experimental results, we find that the system is particularly proficient at calculating the object's center of mass location (Table 1).

There were a number of challenges in the successful utilization of sensor data to traverse the states of the FSM. The simplistic threshold approach in the use of sensor data requires that the thresholds are tuned to this specific system and environment. The accuracy and precision of the data from the ToF are heavily influenced by the ambient lighting conditions, so the ToF was calibrated to lighting that was kept constant throughout all testing, data collection, and operation of the FSM. The appropriate threshold values for the resistive pressure sensors can vary among sensor skins despite using the same circuit design and components, so the values must be calibrated to each sensor skin.

Sensor noise must also be taken into consideration when setting the threshold values. The IMU had particularly noisy data during the transport state and it was difficult to find appropriate threshold values, even after calibrating the magnetometer to the geographic location of the lab and applying a Madgwick filter. The pressure sensors also had abrupt signal fluctuations at periods where the gripper was moving more quickly or changing direction. To address these challenges, we take advantage of the system's multimodal sensing capabilities. The definition of an object grasped by the gripper is driven by a combination of sensor modalities. Of the four available streams of data from the IMU, ToF, and two strain sensors, only three must be in agreement on the presence of the object for decision-making. This reduces the number of incorrect decisions by the FSM caused by sensor noise and threshold value errors.

Another challenge was using image processing techniques with the ToF distance data. Because the 2D array of ToF distance measurements are interpreted as a binary image for the calculation of the object's center of mass, size, and location, it is more susceptible to errors from sensor noise and relies on more assumptions about the objects and environment, compared to a camera sensor with the capability to gather a wider variety of data with potentially higher resolution. However, despite the possibility of increased robustness and more informative data with a camera sensor, we conclude that the ToF provides sufficient resolution and environmental data for use with the control strategy on this system. The ToF offers the advantage of simplicity and allows for a fully integrated sensing solution; the more complex camera sensor is coupled with additional challenges in fabrication and design, and would likely require off-board placement.

The limiting factors on the bandwidth of the system are the speed of the arm in the scanning state and the time required to activate and deactivate the SMA springs in the grasp and release states. In the scanning state, the sampling rate of the sensor skin is approximately 7 Hz, so the arm moves at a speed that is sufficient to achieve the sensor data resolution in the horizontal axis for successful localization of the object. One complete scan of the workspace is obtained in 67s. The time required for the SMA springs to activate

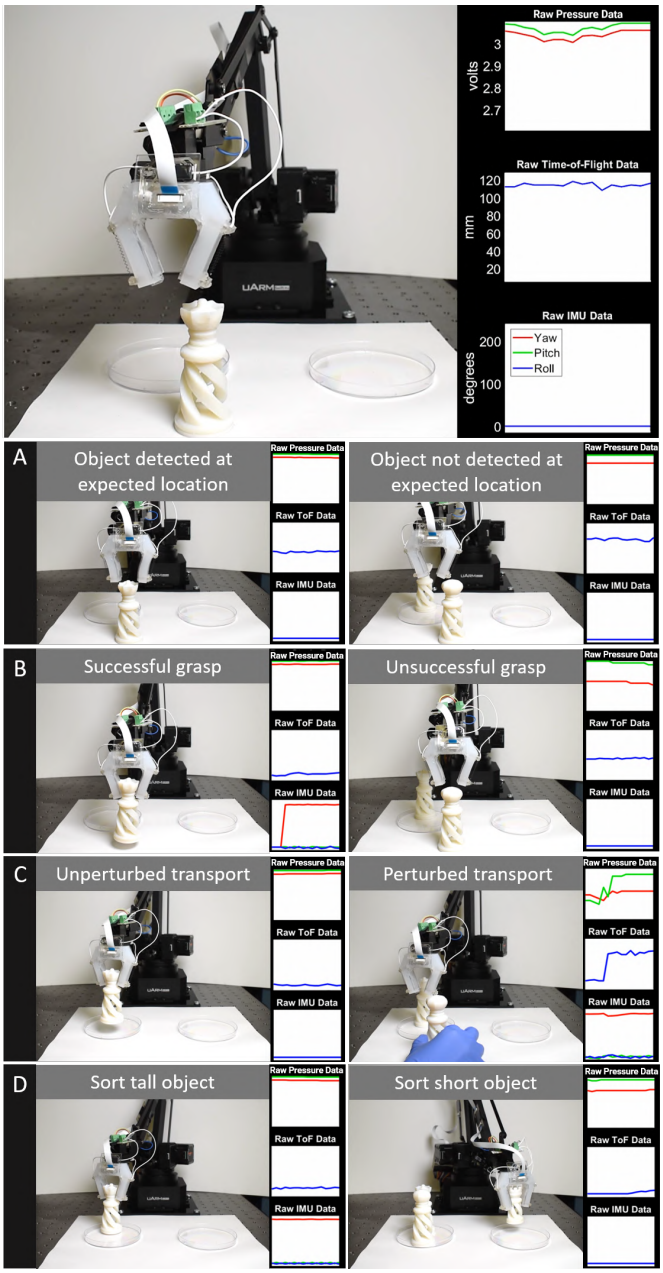

Fig. 5. Comparisons of live sensor data during a complete run of the FSM from A) object detection, B) grasping, C) transport, and D) sorting.

and deactivate is 5s. One complete unperturbed run of the FSM from initialization to the placement of the object in its sorted location is executed in 103s.

VI. DEMONSTRATIONS

The closed-loop control of the soft robotic system is demonstrated in scanning, grasping, and sorting tasks with three 3D printed chess pieces [30] (Objet 24; Stratasys). Two of the chess pieces, the king and the queen, are approximately 25mm in diameter with a height of 80mm, while the rook is approximately 23mm in diameter with a height of 58mm. The dimensions of these chess pieces are within the ranges required for a successful grasp and release from the gripper. The demonstration described below and the data shown in the Figure 5 is from one uninterrupted run of the system.

The demonstration begins with the completely unperturbed scanning, grasping, and sorting of the queen chess piece. The queen chess piece is classified as a tall object with the approximate height of 44mm, as measured by the ToF. The system successfully identifies a valid object within the scanning workspace, moves to the center-of-mass, lowers the gripper to the appropriate height, and grasps it in the first run. The system then moves it to the specified location for tall objects and returns to the scan state.

In the second cycle, external perturbations interfere with the system as it attempts to complete its tasks. After the initial scanning stage is completed, the king chess piece is moved before the gripper reaches the calculated center of mass location (Figure 5A). The system then returns to the scanning state and identifies the king chess piece in its new location. The king chess piece is classified as a tall object with a height of 53mm. The king chess piece remains unperturbed until the gripper attempts to grasp it. The object is held down to prevent a successful grasp and lift (Figure 5B). The distance measurements from the ToF range from 46mm-51mm, greater than the threshold value of 25mm, which assert that the object has not been grasped successfully. In addition, the outputs from the pressure sensors have not decreased by more than 1 Ohm, which would corroborate with the ToF data suggesting that the object is not in the grasp of the gripper. Therefore, the system detects that it has not successfully grasped and lifted the object. It returns to the grasp state and is successful in its second attempt to grasp and lift the object. The arm then begins to move the king chess piece towards the location specified for tall objects. However, the object is removed from the grasp of the gripper before it has been successfully placed in its new location (Figure 5C). The king chess piece is re-positioned within the scanning area of the system, and in the final run with this object, the system is unperturbed and successfully completes the tasks. The execution time for this cycle is 238s.

After the king chess piece is successfully sorted, the rook chess piece is placed in the scanning workspace. The cycle with this object is allowed to proceed unperturbed. The system identifies the rook's center of mass location and correctly classifies it as a short object. The gripper is lowered to the appropriate height to grasp the object, lifts it, and places it in the location for short objects (Figure 5D).

VII. CONCLUSIONS AND FUTURE WORK

In this study, we demonstrated the implementation of closed-loop control of a soft robot system with integrated sensing, processing, decision-making, and actuation. The integration of a finite state machine with a sensorized SMA-actuated soft robot gripper and robot arm demonstrated basic autonomy and sensor feedback control through the tasks of scanning, grasping, and sorting. The successful utilization of a finite state machine validates the potential for applying conventional robotic control strategies to soft robotic systems. A crucial factor in the success of this control strategy is that the soft gripper is designed to behave with low DOF, despite

being fabricated with soft materials and theoretically having infinite degrees of freedom. In this way, the gripper design allows us to circumvent the need for complex mechanical control. Although here the closed-loop control strategy is demonstrated on a soft robot gripper, the same approach can be expanded to other soft robotic systems. If extended to a system with higher DOF, such as a bio-inspired octopus arm, utilization of a more sophisticated mechanical control strategy may be necessary.

Moving forward, we plan to explore the addition of new sensing modalities to enable more avenues of responding to environmental feedback. In addition, we plan to expand this integrated sensing and control strategy to more soft robotic systems, such as a quadruped that moves objects from one location to another in confined environments. With the addition of on-board computing and a battery, advancements could be made towards sensor enabled closed-loop control of untethered soft robots.

ACKNOWLEDGMENT

J.Y. designed the finite state machine, collected data, made the figures, and wrote the manuscript. T.H. fabricated the shape-memory actuated gripper and sensing skin and helped integrate the hardware. All edited the manuscript and figures.

REFERENCES

[1] D. Rus and M. T. Tolley, "Design, fabrication and control of soft robots," *Nature*, vol. 521, no. 7553, pp. 467–475, 2015.

[2] T. George Thuruthel, Y. Ansari, E. Falotico, and C. Laschi, "Control strategies for soft robotic manipulators: A survey," *Soft Robotics*, vol. 5, 01 2018.

[3] H. Wang, M. Totaro, and L. Beccai, "Toward perceptive soft robots: Progress and challenges," *Adv. Science*, vol. 5, no. 9, p. 1800541, 2018.

[4] C. Laschi, B. Mazzolai, and M. Cianchetti, "Soft robotics: Technologies and systems pushing the boundaries of robot abilities," *Sci. Robot*, vol. 1, no. 1, p. eaah3690, 2016.

[5] P. Polygerinos, N. Correll, S. A. Morin, B. Mosadegh, C. D. Onal, K. Petersen, M. Cianchetti, M. T. Tolley, and R. F. Shepherd, "Soft robotics: Review of fluid-driven intrinsically soft devices; manufacturing, sensing, control, and applications in human-robot interaction," *Advanced Engineering Materials*, vol. 19, no. 12, p. 1700016, 2017. [Online]. Available: https://onlinelibrary.wiley.com/doi/abs/10.1002/adem.201700016

[6] K. C. Galloway, K. P. Becker, B. Phillips, J. Kirby, S. Licht, D. Tchernov, R. J. Wood, and D. F. Gruber, "Soft robotic grippers for biological sampling on deep reefs," *Soft Robotics*, vol. 3, no. 1, pp. 23–33, 2016, pMID: 27625917. [Online]. Available: https://doi.org/10.1089/soro.2015.0019

[7] S. R. Shin, B. Migliori, B. Miccoli, Y.-C. Li, P. Mostafalu, J. Seo, S. Mandla, A. Enrico, S. Antona, R. Sabarish, T. Zheng, L. Pirrami, K. Zhang, Y. S. Zhang, K.-t. Wan, D. Demarchi, M. R. Dokmeci, and A. Khademhosseini, "Electrically driven microengineered bioinspired soft robots," *Advanced Materials*, vol. 30, no. 10, p. 1704189, 2018. [Online]. Available: https://onlinelibrary.wiley.com/doi/abs/10.1002/adma.201704189

[8] X. Huang, K. Kumar, M. K. Jawed, A. Mohammadi Nasab, Z. Ye, W. Shan, and C. Majidi, "Highly dynamic shape memory alloy actuator for fast moving soft robots," *Advanced Materials Technologies*, vol. 4, no. 4, p. 1800540, 2019. [Online]. Available: https://onlinelibrary.wiley.com/doi/abs/10.1002/admt.201800540

[9] D. Chen and Q. Pei, "Electronic muscles and skins: a review of soft sensors and actuators," *Chemical reviews*, vol. 117, no. 17, pp. 11 239–11 268, 2017.

[10] N. Lu and D.-H. Kim, "Flexible and stretchable electronics paving the way for soft robotics," *Soft Robotics*, vol. 1, no. 1, pp. 53–62, 2014.

[11] T. Tomo, S. Somlor, A. Schmitz, L. Jamone, W. Huang, H. Kristanto, and S. Sugano, "Design and characterization of a three-axis hall effect-based soft skin sensor," *Sensors*, vol. 16, no. 4, p. 491, 2016.

[12] T. Hellebrekers, O. Kroemer, and C. Majidi, "Soft magnetic skin for continuous deformation sensing," *Advanced Intelligent Systems*, vol. 1, no. 4, p. 1900025, 2019.

[13] W. Li, J. Konstantinova, Y. Noh, Z. Ma, A. Alomainy, and K. Althoefer, "An elastomer-based flexible optical force and tactile sensor," in *2019 2nd IEEE International Conference on Soft Robotics (RoboSoft)*. IEEE, 2019, pp. 361–366.

[14] K. B. Justus, T. Hellebrekers, D. D. Lewis, A. Wood, C. Ingham, C. Majidi, P. R. LeDuc, and C. Tan, "A biosensing soft robot: Autonomous parsing of chemical signals through integrated organic and inorganic interfaces," *Sci. Robotics*, vol. 4, no. 31, p. eaax0765, 2019.

[15] D. H. Ho, Q. Sun, S. Y. Kim, J. T. Han, D. H. Kim, and J. H. Cho, "Stretchable and multimodal all graphene electronic skin," *Advanced Materials*, vol. 28, no. 13, pp. 2601–2608, 4 2016. [Online]. Available: https://doi.org/10.1002/adma.201505739

[16] S. Din, W. Xu, L. K. Cheng, and S. Dirven, "A stretchable multimodal sensor for soft robotic applications," *IEEE Sensors Journal*, vol. 17, no. 17, pp. 5678–5686, Sep. 2017.

[17] J. W. Booth, D. Shah, J. C. Case, E. L. White, M. C. Yuen, O. Cyr-Choiniere, and R. Kramer-Bottiglio, "Omniskins: Robotic skins that turn inanimate objects into multifunctional robots," *Science Robotics*, vol. 3, no. 22, p. eaat1853, 2018.

[18] R. L. Truby, M. Wehner, A. K. Grosskopf, D. M. Vogt, S. G. Uzel, R. J. Wood, and J. A. Lewis, "Soft somatosensitive actuators via embedded 3d printing," *Advanced Materials*, vol. 30, no. 15, p. 1706383, 2018.

[19] R. Li, R. Platt, W. Yuan, A. ten Pas, N. Roscup, M. A. Srinivasan, and E. Adelson, "Localization and manipulation of small parts using gelsight tactile sensing," in *2014 IEEE/RSJ International Conference on Intelligent Robots and Systems*, Sep. 2014, pp. 3988–3993.

[20] T. G. Thuruthel, B. Shih, C. Laschi, and M. T. Tolley, "Soft robot perception using embedded soft sensors and recurrent neural networks," *Science Robotics*, vol. 4, no. 26, 2019. [Online]. Available: https://robotics.sciencemag.org/content/4/26/eaav1488

[21] R. Adam Bilodeau, E. L. White, and R. K. Kramer, "Monolithic fabrication of sensors and actuators in a soft robotic gripper," in *2015 IEEE/RSJ International Conference on Intelligent Robots and Systems (IROS)*, Sep. 2015, pp. 2324–2329.

[22] J. Morrow, H. Shin, C. Phillips-Grafflin, S. Jang, J. Torrey, R. Larkins, S. Dang, Y. Park, and D. Berenson, "Improving soft pneumatic actuator fingers through integration of soft sensors, position and force control, and rigid fingernails," in *2016 IEEE International Conference on Robotics and Automation (ICRA)*, May 2016, pp. 5024–5031.

[23] Y. She, C. Li, J. Cleary, and H.-J. Su, "Design and Fabrication of a Soft Robotic Hand With Embedded Actuators and Sensors," *Journal of Mechanisms and Robotics*, vol. 7, no. 2, 05 2015, 021007. [Online]. Available: https://doi.org/10.1115/1.4029497

[24] H. A. Wurdemann, S. Sareh, A. Shafti, Y. Noh, A. Faragasso, D. S. Chathuranga, H. Liu, S. Hirai, and K. Althoefer, "Embedded electro-conductive yarn for shape sensing of soft robotic manipulators," in *2015 37th Annual International Conference of the IEEE Engineering in Medicine and Biology Society (EMBC)*, Aug 2015, pp. 8026–8029.

[25] J. Zimmer, T. Hellebrekers, T. Asfour, C. Majidi, and O. Kroemer, "Predicting grasp success with a soft sensing skin and shape-memory actuated gripper," in *Proceedings of (IROS) IEEE/RSJ International Conference on Intelligent Robots and Systems*, November 2019.

[26] H. Zhao, K. O'Brien, S. Li, and R. F. Shepherd, "Optoelectronically innervated soft prosthetic hand via stretchable optical waveguides," *Science Robotics*, vol. 1, no. 1, p. eaai7529, 2016.

[27] B. Shih, D. Drotman, C. Christianson, Z. Huo, R. White, H. I. Christensen, and M. T. Tolley, "Custom soft robotic gripper sensor skins for haptic object visualization," in *2017 IEEE/RSJ Int. Conf. on Intelligent Robots and Systems (IROS)*, Sep. 2017, pp. 494–501.

[28] T. Hellebrekers, K. B. Ozutemiz, J. Yin, and C. Majidi, "Liquid metal-microelectronics integration for a sensorized soft robot skin," in *2018 IEEE/RSJ International Conference on Intelligent Robots and Systems (IROS)*. IEEE, 2018, pp. 5924–5929.

[29] K. B. Ozutemiz, J. Wissman, O. B. Ozdoganlar, and C. Majidi, "Egain–metal interfacing for liquid metal circuitry and microelectronics integration," *Advanced Materials Interfaces*, vol. 5, no. 10, p. 1701596, 2018. [Online]. Available: https://onlinelibrary.wiley.com/doi/abs/10.1002/admi.201701596

[30] J. Muirwood and J. Woods, "Spiral Chess Set," *Thingiverse.com*, 07 2015. [Online]. Available: https://www.thingiverse.com/thing:1094870